

Formation of a fine-grained $\text{Si}_{1-x}\text{Ge}_x$ thermoelectric by spark plasma sintering

© M.V. Dorokhin,¹ M.S. Boldin,¹ E.A. Uskova,¹ A.V. Boryakov,² P.B. Demina,¹ I.V. Erofeeva,^{1,¶}
A.V. Zdoroveyshchev,¹ V.E. Kotomina,¹ Yu.M. Kuznetsov,¹ E.A. Lantsev,¹ A.A. Popov,¹ V.N. Trushin¹

¹ Research Institute for Physics and Technology, Lobachevsky State University of Nizhny Novgorod,
603950 Nizhny Novgorod, Russia

² Lobachevsky University of Nizhny Novgorod,
603950 Nizhny Novgorod, Russia

¶ e-mail: irfeya@mail.ru

Received May 21, 2021

Revised August 5, 2021

Accepted August 6, 2021

The kinetics of diffusion processes occurring during the formation of polycrystalline $\text{Si}_{1-x}\text{Ge}_x$ nanostructures ($x = 0.20, 0.35$) by spark plasma sintering in the temperature range 20–1200°C was studied for the first time. A mechanism for the formation of a SiGe solid solution is proposed as a result of a comprehensive study of the microstructure and phase composition of samples with particle sizes from 150 nm to 100 μm, together with the analysis of experimental sintering maps. It is based on the phenomenon of mutual diffusion of Si and Ge atoms that occurs during the entire sintering process. For the selected sintering modes, the grain size of the formed SiGe corresponds to the size of the initial powder particles.

Keywords: spark plasma sintering, solid solution SiGe, thermoelectric characteristics, figure of merit ZT.

DOI: 10.21883/TP.2022.15.55267.152-21

Introduction

Over the last two decades, much attention has been paid to the development and study of nanostructured and fine-grained thermoelectric materials [1–8]. Silicon- and germanium-based compounds — $\text{Si}_{1-x}\text{Ge}_x$ [1,4–7] have a special place among them. They are unique in that Si and Ge, due to an unlimited solubility form a continuous series of substitutional solid solutions with a smoothly changing band gap and obeying the Vegard law of lattice constant [9]. Compared to thermo-electrics from ceramic compounds [2,8], semiconducting SiGe has several advantages: high mechanical strength, radiation and high-temperature stability, low volatility, absence of toxicity and availability of well-established, rather simple production methods. In addition, there is a high level of understanding of electronic properties in bulk $\text{Si}_{1-x}\text{Ge}_x$ in the scientific community.

Nanopolycrystalline thermoelectric $\text{Si}_{1-x}\text{Ge}_x$ is generally prepared from powders either by hot pressing [3,4] or spark plasma sintering (SPS) [5–8]. However, the known publications mainly study the thermoelectric properties of already prepared $\text{Si}_{1-x}\text{Ge}_x$ nanostructures, and the process of material formation during sintering is not considered in detail. Besides widespread is manufacturing of nanopolycrystalline Si–Ge from the powder, obtained by milling prepared material SiGe [4,10], so the study of the mechanism of nano- and finely dispersed solid solution $\text{Si}_{1-x}\text{Ge}_x$ directly in the sintering of Si and Ge powder mixture is, in our opinion, relevant. The SPS method used in this work is unique in its ability to exploit wide

ranges of temperature, pressure and sintering time for the controlled synthesis of various polycrystalline fine grained materials [11]. SPS has recently gained a significant place in technologies for producing thermoelectric materials.

Samples of $\text{Si}_{1-x}\text{Ge}_x$ with germanium content of 20 and 35 at.% were used for the study. The choice of such compositions is related to the problem of improving the thermoelectric characteristics of $\text{Si}_{1-x}\text{Ge}_x$, in particular, reducing the thermal conductivity and increasing the main characteristic parameter for thermoelectrics — the dimensionless thermoelectric quality factor ZT . The value $x = 0.35$ is preferable for use, since it reduces the requirements for the accuracy of the composition of $\text{Si}_{1-x}\text{Ge}_x$: a deviation in the Ge content in either direction by up to 2 at.% does not lead to a significant change in the values of parameters included in ZT [15]. Both compositions — $\text{Si}_{0.65}\text{Ge}_{0.35}$ and $\text{Si}_{0.8}\text{Ge}_{0.2}$ — have quite low thermal conductivity (~ 20 W/m·K) [15]. We emphasize that the trend in recent years is an increasing deviation from the „of the classical“ composition $\text{Si}_{0.8}\text{Ge}_{0.2}$ for thermoelectrics, both in the direction of increasing Ge content and decreasing it. In particularly [13] work can be noted, in which nanostructured silicon was studied, which was characterized by comparable with $\text{Si}_{0.8}\text{Ge}_{0.2}$ values of the thermal conductivity coefficient.

The comprehensive study of the formation mechanism of fine-grained $\text{Si}_{1-x}\text{Ge}_x$ included a detailed study of the experimental sintering maps recorded automatically in real time (t) during spark plasma sintering accompanied with scanning electron microscopy (SEM), X-ray surface microanalysis (XRAM) and X-ray diffraction analysis (XRDA) of

sintered samples. The sintering maps contain the occurring values of current flowing through the graphite mold, voltage between the electrodes, external pressure (press load), heating temperature (T), vacuum level, powder compaction (shrinkage) (L) and shrinkage rate (S) — the first derivative of shrinkage with time. The effectiveness of sintering is indicated by the amount of powder shrinkage — the change in height of the material placed in the mold by the compression and heating forces. The main parameters influencing powder compaction and solid solution synthesis are temperature and process time, therefore, the dependences of T , L and S on time at different sintering–synthesis modes of $\text{Si}_{1-x}\text{Ge}_x$ were considered in this work. Particular attention has also been paid to the conditions, under which the powder is prepared.

1. Experimental procedure

The synthesis of $\text{Si}_{1-x}\text{Ge}_x$ was carried out by sintering a mixture of coarse or fine-grained Si and Ge powders at the SPS DR. SINTER model SPS-625 System in a vacuum of 6 Pa at an applied press pressure of 70 ± 5 MPa between room temperature and 1200°C . The principle of the unit is described in detail in [14]. The heating temperature was monitored by measuring the temperature of the outer surface of the mold with a Chino IR–AHS2 optical pyrometer, according to the plant design starting at $T_{\text{pir}} = 570^\circ\text{C}$. After reaching 570°C (pyrometer on) the heating rate for all samples is $50^\circ\text{C}/\text{min}$ (the rate was controlled by the pyrometer reading). The heating rate is not controlled before the pyrometer is switched on, and the duration of the initial heating may vary from sample to sample. The press pressure was kept constant throughout the sintering process until heating was completed.

The temperature values in the sintering area (T_{sin}) were monitored with a K -type thermocouple as part of the test experiments. According to methods [14,15], the data was converted from the pyrometer reading to the temperature inside the mold using the empirical formula

$$T_{\text{sin}} = 1.215 \cdot T_{\text{pir}} - 73 \text{ K}. \quad (1)$$

The temperature of the sintering process is then taken as the recalculated value T_{sin} from the pyrometer reading.

Material shrinkage was measured with the precision dilatometer included in the unit to an accuracy of $\pm 4 \mu\text{m}$, taking into account the expansion of the mold itself when heating. Note that the amount of shrinkage depends on the mass of sintered powder. Since the powder weights for the different samples differed, the shrinkage value was calculated with a correction factor to make a correct comparison between the samples

$$L = L_d \cdot \mu, \quad (2)$$

where L_d — dilatometer shrinkage reading, $\mu = m_0/m$, m — powder mass, and m_0 — normalization factor — powder

mass № 4, which was 15 g. Here it was taken into account that the shrinkage of the powder is proportional to its mass.

The microstructure, polished surface morphology and grain sizes of the samples were studied on a high-resolution Jeol JSM scanning electron microscope using an X-Max^N 20 (Oxford Instruments) in SED (secondary, low energy electron) or BED (reflected, back-scattered electron) modes. The composition was calculated using the fundamental parameter method implemented on the basis of the micro-analyzing system software. The lines $\text{Si}K_\alpha$, $\text{Ge}K_\alpha$, $\text{Ge}L_\alpha$ were used to determine the composition.

The mixture of powders in given ratios was prepared by milling crumbs of Si and Ge single crystals. The powders were milled on a FRITSCHE Analysette 3 Pro vibratory mill to obtain powders with grain sizes of $50\text{--}100 \mu\text{m}$. For the production of $5\text{--}10 \mu\text{m}$ as well as fine powders after preliminary dry crumb grinding with a FRITSCHE Analysette 3 Pro, the coarse powder was subjected to basic wet grinding in ethanol and inert gas atmosphere Ar in a FRITSCHE Pulverisette 6 planetary mill with grinding balls in a stabilized zirconium dioxide beaker. According to X-ray diffraction analysis, the initial powders were in all cases a mixture of Ge and Si with particle size depending on the milling conditions. The dried powder was also transferred in an argon atmosphere to a graphite mold, which was then placed in the sintering machine. For each value x used, several series of $\text{Si}_{1-x}\text{Ge}_x$ samples were prepared, which differed in powder grain size and sintering conditions, namely, total sintering process duration $700\text{--}900$ s and final sintering temperature $800\text{--}1190^\circ\text{C}$. The time (1.6 h) and speed (150 and/or 250 rpm) of powder milling was varied, in some cases an additional one hour milling at 450 rpm was applied. The milling mode affects the average particle size of powder. The latter was evaluated using electron microscopic images: the average size was calculated by averaging over 200 particle size measurements. A list of the structures investigated is shown in the table below. Samples № 6–10 were made by sintering powder of the same grind, but with varying maximum sintering temperature. This experiment was performed to investigate the structure of the samples at various stages of sintering.

The thermoelectric quality factor ZT is determined by the formula [17]:

$$ZT = \alpha^2 / \rho \lambda \cdot T, \quad (3)$$

where α — Seebeck coefficient, ρ — resistivity, λ — thermal conductivity, T — average temperature.

The Seebeck coefficient was measured by creating a controlled temperature gradient along the structure. The sample is placed on two graphite tables, the heating of which is controlled by temperature controllers. EMF measurement is made using thermocouples attached to the opposite faces of the structure. Thermocouples make it possible to additionally record temperatures on the faces. The resistivity was calculated taking into account the geometric dimensions of the sample based on electrical resistivity measurements.

Parameters of the SPS structures: nominal composition, milling conditions, average particle size of the original powder (a_p), sintered samples density ρ/ρ_0 , maximum sintering temperature (T_{sin}), measured value of the thermoelectric quality factor (ZT)

Sample No	Nominal composition	Conditions milling	$a_p, \mu\text{m}$	ρ/ρ_0	$T_{\text{sin}}, ^\circ\text{C}$	ZT (at $T = 490^\circ\text{C}$)
1	$\text{Si}_{0.8}\text{Ge}_{0.2}$	Vibromill	50–100	0.81	1190	0.08
2	$\text{Si}_{0.65}\text{Ge}_{0.35}$	Vibromill	50–100	0.94	1190	0.07
3	$\text{Si}_{0.8}\text{Ge}_{0.2}$	Vibromill + ball mill	5–10	0.82	1105	0.136
4	$\text{Si}_{0.65}\text{Ge}_{0.35}$	250 rpm, 1 h Vibromill + ball mill	~ 0.5	0.97	1190	0.01
5	$\text{Si}_{0.8}\text{Ge}_{0.2}$	250 rpm, 6 h Vibromill + ball mill	~ 0.5	0.95	1170	—
6	$\text{Si}_{0.65}\text{Ge}_{0.35}$	250 rpm, 6 h Vibromill + ball mill	0.5	0.97	1190	0.54
7	$\text{Si}_{0.65}\text{Ge}_{0.35}$	250 rpm, 6 h Vibromill + ball mill	0.5	0.68	825	—
8	$\text{Si}_{0.65}\text{Ge}_{0.35}$	250 rpm, 6 h Vibromill + ball mill	0.5	0.88	1020	—
9	$\text{Si}_{0.65}\text{Ge}_{0.35}$	250 rpm, 6 h Vibromill + ball mill	0.5	0.92	1140	—
10	$\text{Si}_{0.65}\text{Ge}_{0.35}$	250 rpm, 6 h Vibromill + ball mill	0.5	0.95	1170	—
11	$\text{Si}_{0.65}\text{Ge}_{0.35}$	250 rpm, 6 h +450 rpm, 1 h Vibromill + ball mill	0.15–0.25	0.98	1190	0.63

Note. ρ_0 — density value of single-crystalline $\text{Si}_{1-x}\text{Ge}_x$ with a given composition, calculated from data of work [16]. The density was measured by hydrostatic weighing.

The resistance was measured in a standard four-pin circuit using a Keithley-2400 multimeter calibrator.

The heat transfer coefficient was measured using the steady-state heat flux method. The principle of the method is to compare the heat flux distribution on the investigated structure and on the reference samples. In the experiment, quartz glasses were used as standards.

The measurements were taken in vacuum over a temperature range of 50–500°C. Further thermoelectric measurement techniques can be found in [5–7].

2. Results and discussion

Using the recorded sintering maps, graphs of the time dependences of the EIPC process parameters were plotted. The relations $L(t)$, $S(t)$ and $T(t)$, typical of each milling mode, are shown in Fig. 1, 2. The sintering curves of coarse powder samples with particle sizes 50–100 μm are shown in Fig. 1. For a fine powder with an average particle size

of 0.15–1 μm , the data are shown in Fig. 2. Looking at Figs. 1 and 2 it is seen that, for all the differences, the curves have a common property: the dependences $L(T)$ and $S(T)$ for all structures can be conventionally divided into three temperature intervals by the type of change: I — from room temperature to $600 \pm 30^\circ\text{C}$, II — from 630 to $\sim 950^\circ\text{C}$, III — from 950°C and above, until the end of the process.

2.1. Interval I — from room temperature to 630°C

At low temperatures, the $L(t)$ dependence of all samples shows a slight change in L , indicating that shrinkage is low. The low shrinkage rate is particularly noticeable for samples 1 and 2 (Fig. 1) made from coarse powder (see table).

Electron microscopic images of the surface of these coarse-grained samples show weak mixing of Ge and Si even after sintering at high temperatures. In the case of a coarse-grained sample 3 with an order of magnitude smaller

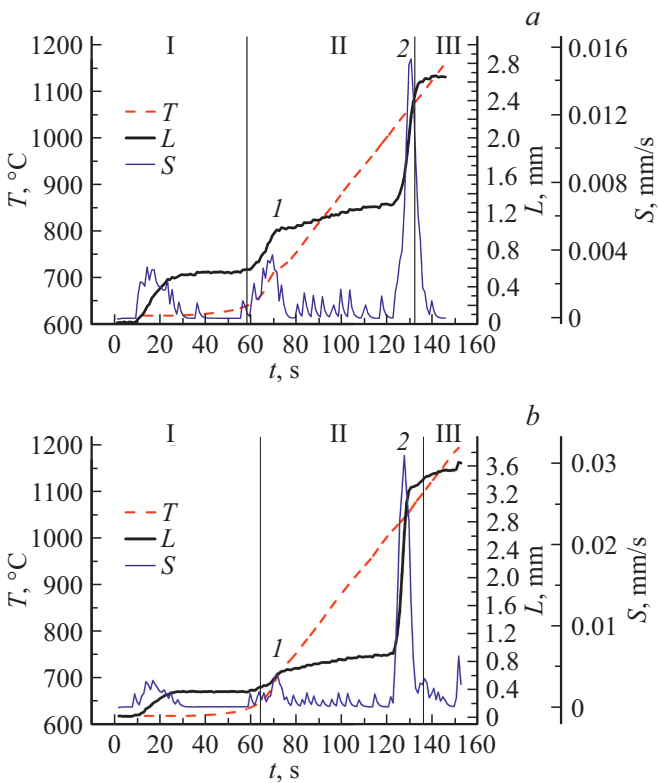


Figure 1. Dependences of temperature, shrinkage and shrinkage rate on time in coarse-grained samples: *a* — № 1, *b* — № 2 (see table).

particle size (see table), the homogeneous mixing of the material during sintering does not occur either. However, as follows from the electron microscopic image (Fig. 3, *a*), along with the priming of Si–Si (dark regions) and Ge–Ge (light regions), the interaction of different particles — silicon and germanium (separate dark grey areas) is observed. It should be noted that the grain size remains the same as in the original powder and a large number of pores (areas of black color) are visible. At the same time, the formed sample is a solid, mechanically strong material. The SEM results are consistent with the X-ray diffraction patterns of the listed samples which, as in the case of the original powder (Fig. 4, *a*), show only single unbound Ge and Si lines.

Thus, the small shrinkage (~ 0.1 mm) in coarse-grained samples at low sintering temperatures can be explained by weak diffusion mixing of Ge and Si particles. The formed low-temperature samples have relatively high resistivity (at $10^3 \Omega \cdot \text{m}$ at room temperature), which seems to be due to the effect of potential barriers on Si/Ge heterojunctions on electronic transport. Due to the high resistivity, the maximum value of ZT for such structures does not exceed $10^{-2} - 10^{-3}$ (see table).

The maximum *I* on the *S* curve at the end point of the I interval (Fig. 1, 2) is an instrumental feature of the sintering unit — pyrometer feedback capture — and is due to the change in current at the exit value $T_{\text{pir}} \approx 570^\circ\text{C}$

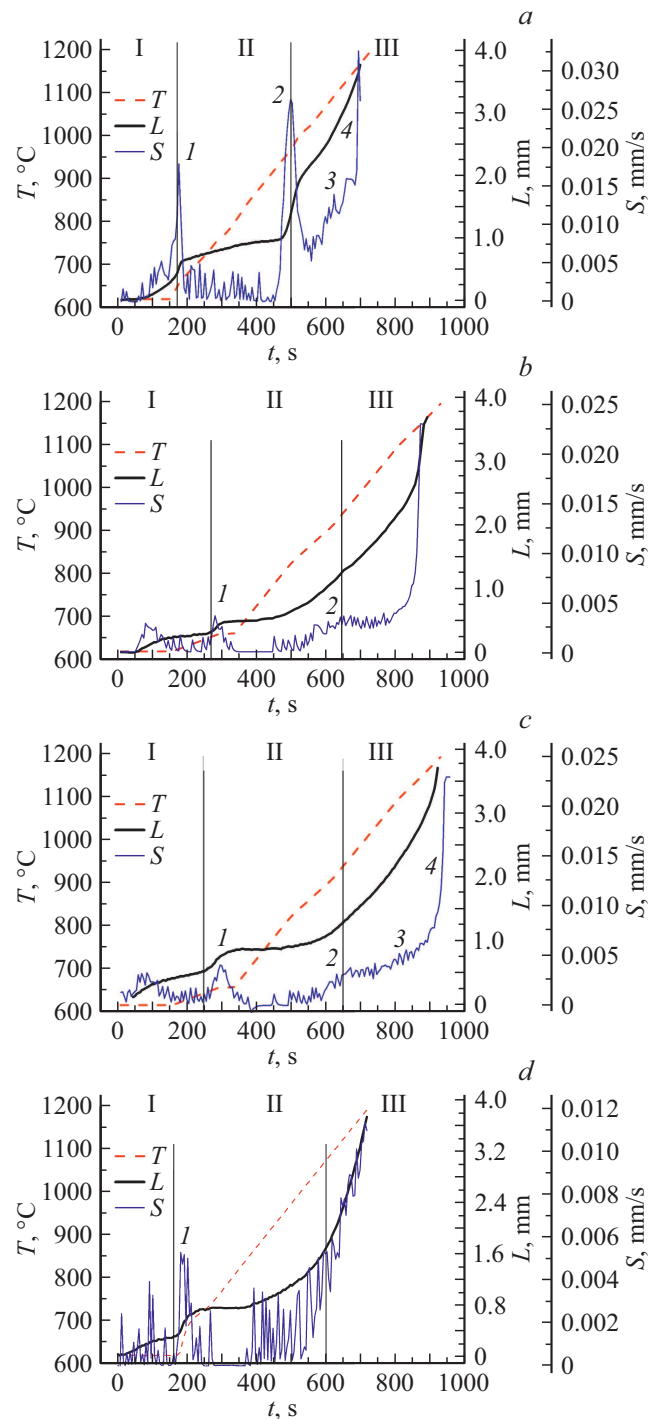


Figure 2. Shrinkage rate time dependencies of the samples: *a* — № 4, *b* — № 5, *c* — № 6, *d* — № 11 (see Table).

when the pyrometer is turned on (in control experiments on thermocouple temperature measurement this maximum is missing).

2.2. Interval II — 630 to 950°C

At temperatures above $\approx 450^\circ\text{C}$, for Ge and $\approx 600^\circ\text{C}$ for Si, any applied pressure creates plastic deformation [18],

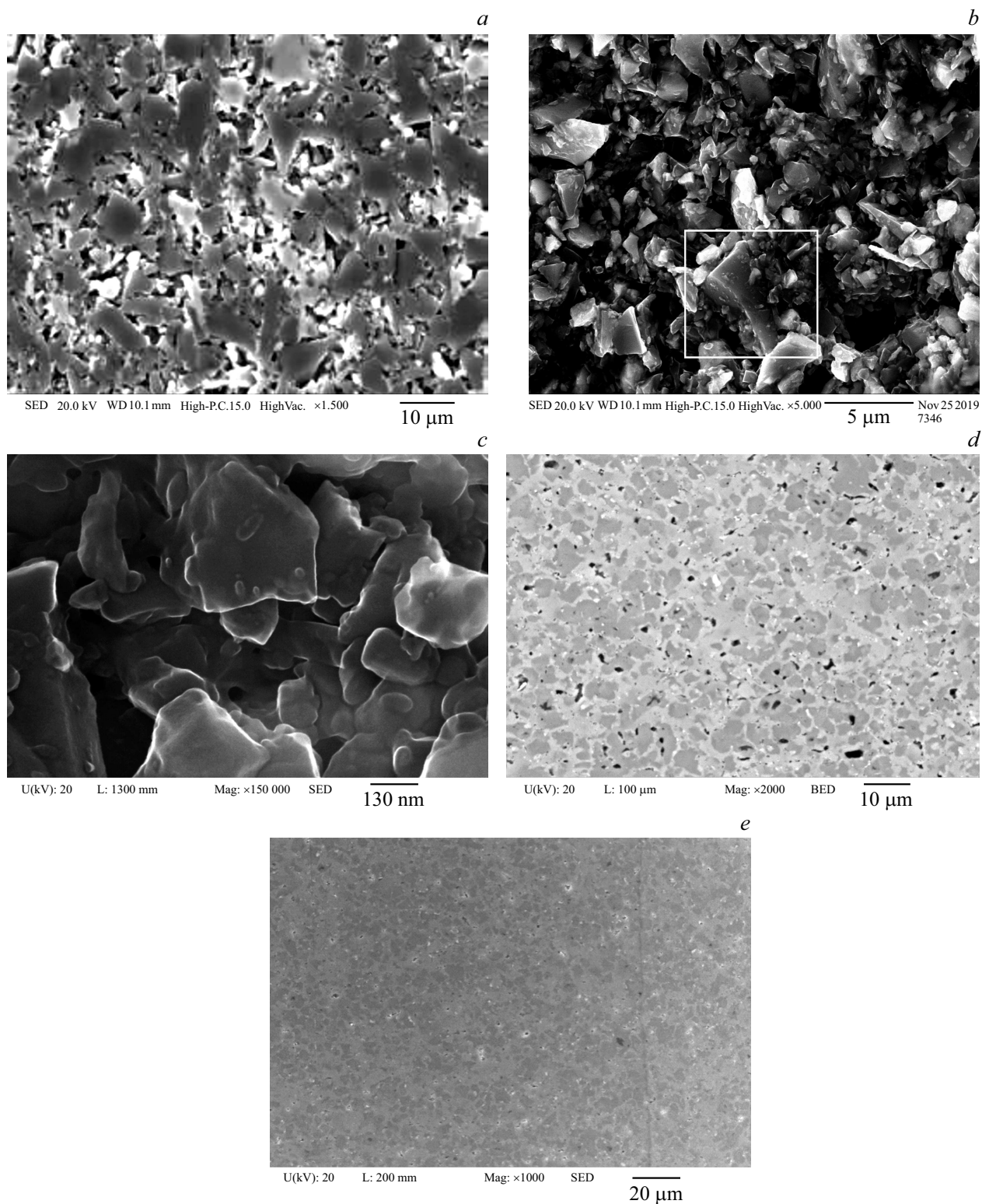


Figure 3. Microscopic image of the sample surface after sintering obtained in SED and BED modes: *a* — № 6, *b* — № 7; *c* — № 9, *d* — № 10; *e* — № 11 (see table). *d* — light gray areas — $\text{Si}_{0.68}\text{Ge}_{0.32}$, dark gray areas — $\text{Si}_{0.89}\text{Ge}_{0.11}$, black — pores; *e* — light gray areas — $\text{Si}_{0.64}\text{Ge}_{0.36}$, dark gray — $\text{Si}_{0.74}\text{Ge}_{0.26}$.

additional dislocation movement and multiplication begins, so in the second temperature interval powder compaction can occur simultaneously and mutually independent by

both atomic diffusion and plastic deformation. Along with diffusion of atoms in the volume and accelerated diffusion along the grain boundaries, grain boundary slip of Ge and

Si particles occurs [19,20]. In total, these factors result in an acceleration of L compared to shrinkage in I interval (Fig. 1 and 2).

According to our theoretical results and results of model experiment on spark sintering of single-crystal Ge and Si [21] plates, solid-phase mutual diffusion of atoms in the diffusion zone in the interval $T = 620\text{--}900^\circ\text{C}$ has accelerated character with activation energies $E_a = 0.33\text{ eV}$ for Ge and $E_a = 0.25\text{ eV}$ for Si. This is an order of magnitude smaller than the values of E_a for bulk diffusion of atoms in a single crystal under ordinary conditions [22], but satisfactory agreement with the parameters of vacancy migration in Ge and Si [22], which is important if one takes into account the vacancy mechanism of mutual diffusion of elements. The penetration depth of Si atoms into germanium is several times greater than for Ge atoms into silicon, according to the results [21]. Transferring these data to the powder material we may conclude that the diffusion of silicon and germanium atoms in the contact area should also have an accelerated character and lead to the formation of a solid solution in the II interval of sintering. Indeed, after sintering at $T_{\text{sin}} = 825^\circ\text{C}$ the formed solid phase $\text{Si}_{1-x}\text{Ge}_x$ with Ge content from 15 to 80 at.% according to XRAM data was found in some local areas of the fine sample (№ 7, see table). An electron microscopic image of this sample (Fig. 3, *b*) shows that many small particles „have baked“ onto larger ones and form conglomerates consisting of 10 particles or more (highlighted in the box, Fig. 3, *b*). They have a variety of mostly elongated polygonal shapes and a wide range in size — from 10–100 nm to several micrometers. The large difference in the size of the nanoparticles apparently accounts for the irregularity of the diffusion front, leading to the large variation found in the SiGe composition. Due to the low volume fraction of the solid solution in the sintered material, the diffraction pattern of the X-ray diffraction analysis still presents only Si and Ge lines (Fig. 4, *b*).

At the final stage of II interval at temperatures approaching $T \approx 930\text{--}950^\circ\text{C}$, a maximum appears in the shrinkage rate curves (Figs. 1 and 2, feature 2). The position of the maximum corresponds well to the melting temperature of germanium $T_{\text{mel}} = 938^\circ\text{C}$ [9], and this allows its presence to be associated with the melting of unbound germanium in solid solution. During melting, there is a stepwise decrease in the specific volume of Ge — phase transition I rod, — which manifests itself in a sharp increase in shrinkage $L(t)$ (Fig. 1, *a, b* and 2, *a*). Then, sintering takes place with the liquid phase.

It is important to note that the presence as well as the magnitude of the maximum $S(t)$ near the melting point of Ge is determined by the particle size of the powder. Particularly strong maxima (feature 2) are characteristic for samples with large particle sizes (Fig. 1). This is evidently due to the relatively small interaction between Ge and Si in these samples at low temperatures, as shown above, with the result that much of the germanium is not bonded to silicon in a solid solution.

A significant reduction in particle size ($< 250\text{ nm}$, sample № 11, see table) changes the mixing conditions of Ge and Si in the sintering process. In this case, most of the Ge and Si particles are dissolved into each other, so the value of the characteristic peak it2 on the $S(t)$ curve at the II and III intervals decreases significantly (Fig. 2, *d*).

The larger-than-sample № 11 average size ($\sim 500\text{ nm}$) of the powder particles appears to be a borderline situation, where the appearance of a maximum on $S(t)$ is determined by the proportion of undissolved Ge: when the proportion is high enough it is observed (Fig. 2, *a*), while a relatively low proportion is — absent (Fig. 2, *b, c*). For these structures, the presence of a maximum it2 depends not only on the particle size fluctuations, but mainly on the heating regime. For example, the difference between samples № 4 and № 6 under otherwise equal conditions (see table) is the cumulative sintering time in I and II intervals (Fig. 2, *a* and *c* for samples № 4 and № 6, respectively). At fast, especially in the I interval, heating (450 s for the sample № 4) fewer germanium particles may have time to establish diffusion contact with Si and the Ge melting occurs more intensively (Fig. 2, *a*). At prolonged initial heating (650 s for the sample № 6) on the $S(t)$ dependences the feature 2 is smoothed (Fig. 2, *c*), which indicates a low content of free Ge. The above considerations are in agreement with the sintering results of a № 5 sample of different composition (see table) but with the same particle size and also sintered for 650 s (before the end of the II interval). For this sample, the maximum 2 on the $S(t)$ dependence is also absent (Fig. 2, *b*).

In measurements of thermoelectric parameters of $\text{Si}_{1-x}\text{Ge}_x$, it was found [7] that they have the best values with long duration I and II periods with diffusion mixing Si and Ge. Thus, for the same particle size, the duration of the initial sintering periods plays an important role in the solid-phase formation of thermoelectric SiGe.

2.3. Interval III — from 950°C and up

In interval III, an increased shrinkage is observed, which corresponds to sintering involving the liquid phase of molten Ge and the resulting solid solution $\text{Si}_{1-x}\text{Ge}_x$. The composition and state of the latter is determined by the transition temperature of Si through the solidus curve of the Ge–Si [9] phase diagram.

In the presence of the liquid phase, on the one hand, the movement of the solids relative to each other is facilitated, allowing the creation of new contact surfaces Si and Ge. On the other hand, the rate of self and hetero-diffusion of atoms increases significantly. Both factors accelerate the formation of solid solution [23,24] and develop a material shrinkage process with increasing temperature (Fig. 2, interval III).

When sintered to a maximum temperature of 1020°C (sample № 8), approximately equal to 0.85 of the melting temperature (T_{mel}) of $\text{Si}_{0.65}\text{Ge}_{0.35}$, the germanium is completely consumed in the formation of a solid solution, which is confirmed by the absence of separate lines associated

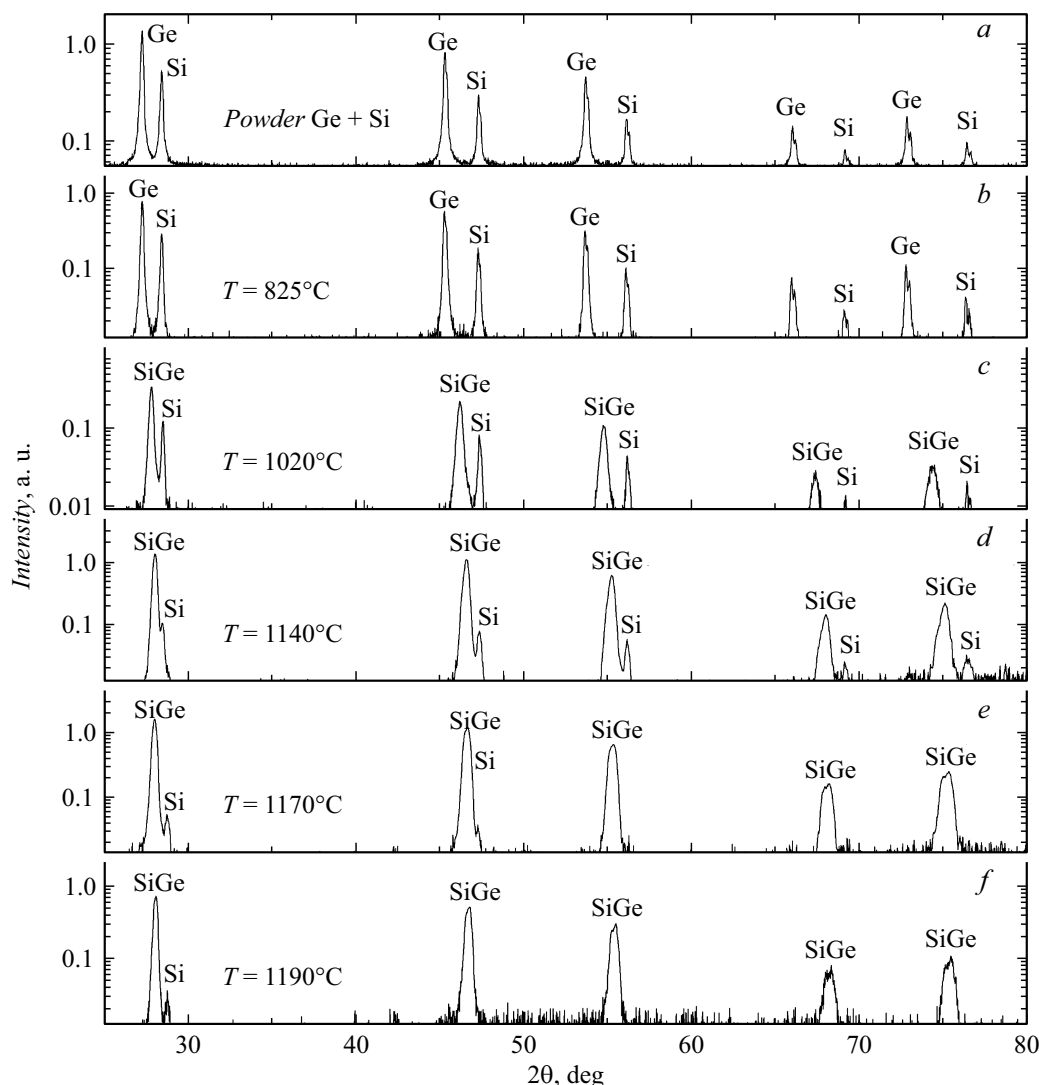


Figure 4. X-ray diffraction spectra of Si–Ge structures formed at different values of maximum sintering temperature: *a* — initial powder after grinding before sintering, *b–f* — samples № 7–11 (see table).

with Ge on the radiographs; besides, the solid solution line $\text{Si}_{1-x}\text{Ge}_x$ appears on the radiograph for the first time (Fig. 4, *c*). The Si-related lines are still fixed, but their intensity decreases as the maximum sintering temperature increases and the SiGe lines shift towards increasing silicon content (Fig. 4, *d, e*). At $T_{\text{sin}} = 1190^\circ\text{C}$, the silicon line intensity is at the detection threshold (Fig. 4, *f*): the material as a result of mutual diffusion is an entirely solid solution.

The XRDA results agree well with the electron microscopic images: in the high-temperature samples with $T_{\text{sin}} = 1140\text{--}1170^\circ\text{C}$ the $\text{Si}_{1-x}\text{Ge}_x$ grains have a complex shape with „smoothed“ corners (Fig. 3, *cV*). This indicates that the solid solution grains have a greater diffusion interaction with each other and with the silicon particles than in the II interval and that a liquid phase of $\text{Si}_{1-x}\text{Ge}_x$ is present at the moment of sintering (Fig. 3, *d*).

The temperature 1140°C is near the value of $0.85T_{\text{mel}}$ of silicon, at which the formation of the sintered material structure is complete [19]. In sample № 9 sintered to $T_{\text{sin}} = 1140^\circ\text{C}$, the formation of two solid solution

compositions was found: the formed $\text{Si}_{1-x}\text{Ge}_x$ has phases with $x = 0.40 \pm 0.01$ and 0.18 ± 0.01 according to XRAM. After sintering to 1190°C , it is found that the material (sample № 6) consists of discrete phases $\text{Si}_{0.64}\text{Ge}_{0.36}$ and $\text{Si}_{0.74}\text{Ge}_{0.26}$ (Fig. 3, *e*). Analysis of the fine structure of the XRDA line of this sample showed that it can be represented as a sum of two components corresponding to SiGe with slightly different compositions. There are no phases with „intermediate“ x . This corresponds to the diagram of the Ge–Si system for the case of non-equilibrium, as in our experiment, cooling down of the material after sintering.

It can be assumed that the formation of SiGe solid solution of two discrete compositions is a characteristic property of the material formed by SPS from fine powder. The high maximum sintering temperature causes solid solutions to remain in two phase states during sintering — liquid and solid. For example, at 1190°C , the material composition $\text{Si}_{0.64}\text{Ge}_{0.36}$ with $T_{\text{sin}} = 1180^\circ\text{C}$ is in a liquid state, and the material $\text{Si}_{0.74}\text{Ge}_{0.26}$ with $T_{\text{mel}} = 1237^\circ\text{C}$ — in a solid one.

This assumption is confirmed by the fact that at temperatures above $T = 1140^\circ\text{C}$, in some cases, the mechanical stability of the system is lost, and an additional abrupt change in the linear dimensions of the sample begins, caused in particular by partial extrusion of the sintered material from the mold; in this interval the largest change of L is observed during the whole sintering time.

An increase in the sintering limit temperature simultaneously leads to a further reduction in the number of pores (cf. Fig. 3, *d* and *e*) and very rapid shrinkage (Fig. 2, section 4). The high temperature samples have quite high relative density (~ 0.97) and good thermoelectric parameters: the Seebeck coefficient $\approx 490\ \mu\text{V/K}$, conductivity $\approx 10^4\ \Omega^{-1}\cdot\text{m}^{-1}$, thermal conductivity $\approx 2.7\ \text{W/m}\cdot\text{K}$, the maximum value obtained ZT is 0.63 (at a measurement temperature of 490°C) [7].

Conclusion

Thus, as a result of the complex analysis of the compaction kinetics of Si–Ge powders mixture during spark plasma sintering and the data of X-ray diffractometry and electron microscopy of sintered samples, the mechanism of nano- and finely dispersed solid solution $\text{Si}_{1-x}\text{Ge}_x$ was considered. The mechanism is based on the phenomenon of mutual diffusion of silicon and germanium atoms, depending on the temperature interval of sintering in the solid or liquid phase.

It was found that the structure and phase composition of the formed $\text{Si}_{1-x}\text{Ge}_x$ are related to the uniformity of components mixing in the sintering process, which in turn depends on the powder dispersion, the maximum sintering temperature and the total duration of the process. Such a detailed study of the processes occurring during SPS of semiconductor materials has been carried out for the first time.

Acknowledgments

The authors would like to thank Prof. V.N. Chuvildeev and Dr. A.V. Nokhrin for helpful discussion of the results.

Funding

This work was supported by the Russian Foundation for Basic Research (Projects 20-38-70063 and 20-32-90032-Aspirants).

Conflict of interest

The authors declare that they have no conflict of interest.

References

- [1] Bo Yu, M. Zebajjadi, H. Wang, K. Lukas, H. Wang, D. Wang, C. Opeil, M. Dresselhaus, G. Chen, Z. Ren. *Nano Lett.*, **12**, 2077 (2012).
- [2] L.P. Bulat, L.V. Bochkov, I.A. Nefedova, R. Akhiska. *Scientific and Technical Bulletin of Information Technology, Mechanics and Optics*, **4** (92), 48 (2014).
- [3] N. Mingo, D. Hauser, N.P. Kobayashi M. Plissonnier, A. Shakouri. *Nano Lett.*, **9**, 11 (2009).
- [4] D.A. Ovsyannikov, M.Y. Popov, S.G. Buga, A.N. Kirichenko, S.A. Tarelkin, V.V. Aksenonenkov, E.V. Tatyaniin, V.D. Blank. *FTT*, **57** (3), 590 (2015).
- [5] I.V. Erofeeva, M.V. Dorokhin, A.V. Zdoroveishev, Y.M. Kuznetsov, A.A. Popov, E.A. Lantsev, A.V. Boryakov, V.E. Kotomina. *FTP*, **52** (12), 1455 (2018).
- [6] M.V. Dorokhin, P.B. Demina, I.V. Erofeeva, A.V. Zdoroveishev, Y.M. Kuznetsov, M.S. Boldin, A.A. Popov, E.A. Lantsev, A.V. Boryakov. *FTP*, **53** (9), 1182 (2019).
- [7] M.V. Dorokhin, P.B. Demina, I.V. Erofeeva, A.V. Zdoroveishev, Y.M. Kuznetsov, E.A. Uskova, M.S. Boldin, E.A. Lantsev, A.A. Popov, V.N. Trushin. *Materials of XXIV Int. Symp. „Nanophysics and Nanoelectronics“* (Nizhny Novgorod, Russia, 2020), vol. 2, p. 551.
- [8] V.A. Kulbachinsky. *Russian Nanotechnology*, **14** (7–8), 30 (2019). DOI: 10.21517/1992-7223-2019-7-8-30-42.
- [9] M.G. Kekua, E.V. Khutsishvili. *Solid solutions of the germanium–silicon semiconductor system* (Metsniereba, Tbilisi, 1985).
- [10] J. Han, T. Jiang, J. Li, Y. Xiang. *Method for preparing SiGe thermoelectric*. CN 108258110 A (China, 2018).
- [11] M. Tokita. In *Handbook: Advanced Ceramics* (Academic Press, 2013), Chapter 11.2.3, p. 1149.
- [15] H. Stöhr, W. Klemm. *Anorgang. Algem. Chem.*, **241** (4), 305 (1939).
- [13] P.K. Gogna, J.P. Fleurial, S.K. Bux, R.B. Kaner, R.G. Blair, H. Lee, G. Chen, M.S. Dresselhaus. *J. Adv. Functional Mater.*, **19**, 2445 (2009).
- [14] M.S. Boldin. *Dissertation. kinetics of electropulse plasma sintering of aluminum oxide ceramics* Candidate of Physical and Mathematical Sciences (Nizhny Novgorod, N.I. Lobachevsky NNSU, 2019).
- [15] V.N. Chuvildeev, M.S. Boldin, Ya.G. Dyatlova, V.I. Rummyantsev, S.S. Ordanyan. *Journal of Inorganic Chemistry*, **60**(8), 1088 (2015).
- [16] F. Schaffler, in *Properties of advanced semiconductor materials GaN, AlN, InN, BN, SiC, SiGe* (John Wiley & Sons, Inc., NY, 2001), p. 149.
- [17] C. Gayner, K.K. Kar. *Prog. Mat. Scienc.*, **83**, 330 (2016).
- [18] R.G. Rodes. *imperfections and active centers in semiconductors*, translated from Eng. edited by S.S. Gorelik. (Metallurgiya, M., 1968)
- [19] B.A. Kalin. *Physical Materials Science*, under the general editorship of B.A. Kalin. Vol 4. E.G. Grigoryev, Y.A. Perlovich, G.I. Solovyov *Physical Bases of Strength. Radiation physics of solids. Computer modelling* (MEPhI, Moscow, 2008)
- [20] Ya.E. Geguzin. *Sintering Physics* (Nauka, M., 1984)
- [21] Yu. Kuznetsov, M. Bastrakova, M. Dorokhin, I. Erofeeva, P. Demina, E. Uskova, A. Popov, A. Boryakov. *AIP Advances*, **10**, 065219 (2020) DOI:10.1063/5.0011740
- [22] H.H. Silvestri, H. Bracht, J. Lundsgaard Hansen, A. Nylandsted Larsen, E.E. Haller. *Semicond. Sci. Tech.*, **21**, 758 (2006). <http://doi.org/10.1088/0268-1242/21/6/008>
- V.A. Ivensen. *Sintering phenomenology and some questions of theory* (Metallurgy, M., 1985)
- [24] W.J. Huppmann. In: Kuczynski G.C. (eds) *Sintering and Catalysis. Materials Science Research* (Springer, Boston, 1975), v. 10, p. 312.